

**REAL TIME MONITORING OF HIGH INTENSITY FOCUSED ULTRASOUND
LESION FORMATION USING ACOUSTO-OPTIC SENSING**

PUXIANG LAI,^{*} JAMES R. MCLAUGHLAN,^{*} ANDREW B. DRAUDT,^{*} TODD W.
MURRAY,[†] ROBIN O. CLEVELAND,^{*} AND RONALD A. ROY^{*}

^{*}Department of Mechanical Engineering, Boston University, Boston, MA, USA; and

[†]Department of Mechanical Engineering, University of Colorado at Boulder, Boulder, CO, USA

Corresponding authors:

Puxiang Lai

Boston University, Department of Mechanical Engineering

110 Cummington Street, Boston, MA 02215 USA

1-857-225-0962

laipuxiang@gmail.com

Ronald A. Roy

Boston University, Department of Mechanical Engineering

110 Cummington Street, Boston, MA 02215 USA

1-617-353-4846

ronroy@bu.edu

Abstract

High intensity focused ultrasound (HIFU) is a promising modality that is used to non-invasively ablate soft tissue tumors. Nevertheless, real-time treatment monitoring with diagnostic ultrasound still poses a significant challenge since tissue necrosis, in the absence of cavitation or boiling, provides little acoustic contrast with normal tissue. In comparison, the optical properties of tissue are significantly altered accompanying lesion formation. A photorefractive crystal-based acousto-optic (AO) sensing system that uses a single HIFU transducer to simultaneously generate tissue necrosis and pump the AO interaction is used to monitor the real-time optical changes associated with thermal lesions induced in chicken breast *ex vivo*. It is found that the normalized change in AO response increases proportionally with the volume of necrosis. This study demonstrates AO sensing can identify the onset and growth of lesion formation in real time and, when used as feedback to guide exposures, results in more predictable lesion formation.

Key Words: High intensity focused ultrasound, Lesion formation, Monitoring, Guidance, Acousto-optic imaging, Photorefractive crystal, Lesion volume, Active and passive cavitation detection

INTRODUCTION

Monitoring of high intensity focused ultrasound (HIFU) treatment

High intensity focused ultrasound (HIFU) is a promising non-invasive technique that is used to induce thermal damage of soft tissue tumors, while minimizing damage to outlying regions (ter Haar 1995). The thermal damage, or tissue necrosis generated by HIFU exposures, is commonly referred to as a “lesion”. Presently, HIFU has been investigated for many applications, such as haemeostasis (Vaezy *et al.* 1998), thrombolysis (Rosenschein *et al.* 2000), drug/gene delivery (Porter and Xie 2001; Ng and Liu 2002), and the treatment of tumors in liver (ter Haar *et al.* 1989; Kennedy *et al.* 2004), kidney (Vallancien *et al.* 1993; Kohrman *et al.* 2002; Wu *et al.* 2003b), prostate (Gelet *et al.* 2000; Uchida *et al.* 2002; Thuroff *et al.* 2003), uterus (Chan *et al.* 2002; Stewart *et al.* 2003), breast (Gianfelice *et al.* 2003a; Wu *et al.* 2003a), and pancreas (Wu *et al.* 2005; Xie *et al.* 2008).

The different physical properties of tissue layers in the acoustic path between the transducer and the focal region, however, limit the reliability in estimating the HIFU intensities *in situ* (Maleke and Konofagou 2008). This, along with uncertainty in the degree of tissue cooling from blood flow, serves to complicate treatment planning. In order to improve the efficacy and safety of HIFU treatment there is a need for reliable real-time monitoring techniques that correspond to the lesioned tissue *in situ*. This would allow for the implementation of precise protocols to provide the optimum treatment of the tumourous region (Rivens *et al.* 2007). A number of non-invasive techniques have been developed to tackle this problem such as magnetic resonance imaging (MRI) (Cline *et al.* 1993; Gianfelice *et al.* 2003a), diagnostic ultrasound (ter Haar *et al.* 1989; Illing

and Chapman 2007), magnetic response elastography (MRE) (Lewa 1991), radiation force elastography (RFE) (Lizzi *et al.* 2003) and vibroacoustography (Konofagou *et al.* 2003). Among these, MRI and diagnostic ultrasound are the only methods that are currently used clinically.

MRI has been used to delineate tissue types and map the temperature change resulting from HIFU exposures with millimeter spatial and 2°C temperature resolution *in vivo* (Tempany *et al.* 2003; Rivens *et al.* 2007). MRI is currently the “gold standard” for HIFU guidance (Cline *et al.* 1993; Hynynen *et al.* 1996; McDannold *et al.* 1998; Furusawa *et al.* 2006) and has been used clinically in the treatment of breast carcinoma (Gianfelice *et al.* 2003b) and uterine fibroids (Stewart *et al.* 2003). A significant disadvantage of this imaging technique, which is particularly pertinent for temperature imaging, is that each image frame can take up to several seconds to acquire (Vaezy *et al.* 2001; Kopelman *et al.* 2006), which may not be fast enough for real-time monitoring. Furthermore, the high cost of the apparatus, the lack of portability, and requirement for a magnetically compatible HIFU system further increases the design complexity and cost, ultimately limiting the accessibility of this modality (Kennedy 2005). Conversely, diagnostic ultrasound is comparatively inexpensive, portable, and capable of imaging in real time with reasonable spatial resolution. Ultrasound-guided HIFU has been implemented clinically, for both extracorporeal (Wu *et al.* 2004; Wang *et al.* 2009) and transrectal (Uchida *et al.* 2002; Illing and Chapman 2007) treatments. When using diagnostic imaging in conjunction with HIFU, it is necessary to temporally interleave the imaging and therapy beams in order to avoid acoustic interference in the B-mode images (Vaezy *et al.* 2001). However, insufficient acoustic contrast between necrotic and normal

tissue results in the inability to reliably visualize lesions on B-mode images (Hill and ter Haar 1995) unless the exposure possesses the intensity and duration needed to generate actual boiling within the lesion, leading to a hyperechoic response (Vaezy *et al.* 2001; Rabkin *et al.* 2005; Rabkin *et al.* 2006; Coussios *et al.* 2007). Studies (Meaney *et al.* 1998; Meaney *et al.* 2000; Bailey *et al.* 2001; Khokhlova *et al.* 2009) show that cavitation and/or boiling may alter the lesion location, shape and size. Furthermore, the formation of cavitation and/or boiling is hard to predict and control. More importantly, bubbles and lesions do not necessarily coincide (Rivens *et al.* 2007).

Acousto-optic imaging (AOI)

The sensing contrasts of the modalities discussed above are based on the dynamic changes in either proton resonant frequency or mechanical/acoustic properties accompanying the thermal necrosis of tissue. In soft tissue, such as liver and breast, thermal necrosis induces an increase in the optical absorption coefficient (μ_a) and the reduced scattering coefficient (μ'_s) of the lesioned volume. In the visible and near-infrared (NIR) optical wavelength range, optical absorption in tissue is predominantly dictated by the relative concentrations of water, lipids, oxy-haemoglobin (HbO₂) and deoxy-haemoglobin (Hb) (Quaresima *et al.* 1998), and scattering is affected by tissue structural inhomogeneities and variations in index of refraction. A study from Nilsson *et al.* (1998) demonstrated 100-300% increase in optical absorption and 120-280% increase in reduced scattering coefficient (for 600-1500 nm) in necrotic and normal rat liver *in vivo*. Similar trends were reported for *ex-vivo* porcine liver (Khokhlova *et al.* 2006) and chicken breast (Ben-David *et al.* 2008) at wavelengths of 1064 and 1041 nm, respectively.

Three major mechanisms have been proposed for the observed increases in optical absorption and scattering. First, the coagulation increases the concentration of chromophores (Cilesiz and Welch 1993; Yaroslavsky *et al.* 2002). Next, the formation of methemoglobin from haemoglobin during blood coagulation has been shown (Black and Barton 2004) to cause a five-fold increase in the absorption at 1064 nm. Finally, the decrease in the average effective size of the scatterers further increases the number of scattering sites and consequentially the scattering (Nilsson *et al.* 1998).

Optical sensing, therefore, presents a potential modality for monitoring lesion formation in tissues such as breast, brain, and prostate, where optical access is facilitated by characteristically low absorption, particularly when compared with highly vascularized tissues such as kidney and liver. However, light is highly scattered in most biological tissues, resulting in a diffusive optical field that limits spatial resolution to approximately 5 mm (at best) for penetration depths of order centimeters (Boas *et al.* 2001). Focused ultrasound has been used to phase modulate diffuse light (Dolfi and Micheron 1989; Marks *et al.* 1993; Wang *et al.* 1995) in an effort to realize the detection of optical contrast deep within tissue with sub-millimeter spatial resolution. This hybrid technique is referred to as acousto-optic imaging (AOI), or ultrasound-modulated optical tomography (UMOT). In AOI tissue is exposed to continuous wave (CW) or pulsed light and sound simultaneously. Light is diffused in the sample, and individual photons that are propagating along different optical paths can either be absorbed or scattered. The presence of the ultrasound results in a dynamic displacement of the scattering sites causes a change to the optical path length and an associated phase shift in the light propagating along a given path. The ultrasound field also affects the refractive index and this too can

alter the optical path length and lead to a phase shift. These two mechanisms (Leutz and Maret 1995; Wang 2001) and their interaction (Sakadzic and Wang 2005) result in a net phase shift of the light collected outside of the sample (Murray and Roy 2007). This process is generally referred to as the ultrasound modulation (or ‘tagging’) of diffuse light. Both modulation depth and the flux of modulated photons are indicative of the strength of this acousto-optic (AO) interaction within the sensing volume, which in turn is sensitive to tissue optical properties (Murray *et al.* 2004; Ramaz *et al.* 2004; Sakadzic and Wang 2004). As this AO interaction only occurs when and where light and sound coexist, the spatial resolution of this “acoustically pumped optical sensor” is dictated by the intersection of the light and sound fields and typically this is governed by the ultrasound beam, for example, using a focused megahertz ultrasound beam can yield AO imaging with sub-millimeter resolution.

Acousto-optic imaging is a relatively new technique that has yet to be employed in a clinical setting, largely because the very weak fluxes of modulated photons generated at deeper depths call for extended sampling times in order to achieve an adequate signal to noise ratio (SNR). The further requirement that the ultrasound beam be spatially scanned leads to 2-D image acquisition times of order minutes (Bossy *et al.* 2005), hardly a real time imaging modality. However, this limitation is less restrictive in the case of AO *sensing* of a fixed volume, where scanning of the ultrasound beam is not necessary. In this paper, AO sensing at NIR wavelength is used to monitor, in real time, the formation of *non-cavitating* lesions from HIFU exposures in excised chicken breast. The formation of a lesion results in a measurable increase in both the optical absorption and the reduced scattering coefficients, which in turn induces a reduction in the amplitude of

the AO signal level. The sensing technique is based on an AOI system developed previously (Sui *et al.* 2005; Lai *et al.* 2009) and modified to allow for real-time monitoring of a fixed volume using a lock-in amplifier to enhance the SNR. Since the same HIFU beam is used to simultaneously form the lesion and pump the AO response, registration between the sensing and therapy modalities is automatic and the system is used to both monitor the onset of lesion formation and estimate the resulting lesion volume in real time.

MATERIALS AND METHODS

Figure 1 is a schematic depiction of the experimental apparatus used for this study. It is comprised of four sub-systems: a HIFU system to provide both the local heating and ultrasound modulation; a GaAs photorefractive crystal-based AO sensing system operating at NIR wavelength to detect the local optical properties of the tissue; a B-mode ultrasound imaging system; and a passive cavitation detection system using a single element transducer.

Sample preparation

Ex-vivo chicken breast (labeled “Sample” in Figure 1) was used for this study. Tissue samples were purchased 24 hours prior to the experiment from a local grocery store. The tissue samples were cut from the chicken breasts to a size of 50x50 mm along both the X and Z axes and 15-30 mm along the Y axis (see Figure 1). The tissue samples were degassed in 1% phosphate buffered saline solution (PBS, BP665-1, FisherBiotech, NJ, USA) for three hours (Aspirator Pump, Model 7049-00, Cole-Parmer Instrument

Company, Ill, USA). The sample was then mounted in an acrylic holder that was designed to hold the tissue through gentle compression in the Y direction using two plates positioned in the X-Z plane. The sample and holder were then submerged in an acrylic tank (400x180x160 mm³) filled with freshly degassed (1 hour) water. The holder was attached to a three-dimension automated translation stage (VXM, Velmex, NY, USA) that allowed the sample to be positioned accurately with respect to the HIFU focus.

In this study, two or three lesions were produced in each sample, with a minimum separation of 10 mm along the Z-axis between neighboring lesions. The focal peak of the HIFU was approximately 16 mm into the tissue along the X axis. To ensure that subsequent lesions are generated from the same initial conditions, a minimum of three minutes wait time was used between exposures to allow for tissue cooling. In addition, a thermometer was used to monitor the water temperature at two hour intervals for each experiment, yielding a mean value of $21 \pm 2^{\circ}\text{C}$.

HIFU exposure sub-system

A function generator (33120A, Agilent, CA, USA), programmed by a personal computer (Dimension 4600, Dell, TX, USA), generated a 1.1 MHz sine wave that was 100% amplitude modulated using a 50 Hz square wave, yielding a pulse train possessing a 50% duty cycle. The output of the function generator was attenuated 20 dB before being sent to a power amplifier (55dB, A150, ENI, NY, USA), whose output was connected to an impedance matching network. The output of the impedance matching network was monitored with a high-impedance voltage probe, which was connected to an oscilloscope (LC334A, LeCroy, NY, USA) and served as an indicator of HIFU pressure

amplitude. In a separate measurement performed in degassed water, the driving voltage into the HIFU transducer was mapped to acoustic pressure at the focus using a calibrated fiber optic probe hydrophone (100 μm fiber diameter, FOPH500, RP Acoustics, Leutenback, Germany). A 70-mm aperture, spherically focused single-element piezoelectric transducer (H102, Sonic Concepts, WA, USA) with a 20-mm diameter central hole served as the HIFU source. The acoustic beam profile was measured at a peak positive pressure of 9.5 MPa and the 6 dB full width half maximum (FWHM) of the focal region was measured to be $10.5 \times 1.6 \times 1.6 \text{ mm}^3$. The acoustic axis of the HIFU transducer was aligned perpendicular to the incident laser beam such that the focal point intersected with the center of the laser beam.

Table 1 details the exposure parameters used in this study. The acoustic intensities were chosen in order to necrose tissue while avoiding the generation of inertial cavitation and/or boiling. Two study groups were used to explore how the AO response change is related to lesion formation under the same (Group 1) or different (Group 2) exposure parameters. The exposures in a third category (Group 3) were used to investigate the feasibility of using the AO response to dynamically guide the exposure duration in order to obtain more consistent and repeatable lesion volumes compared with exposures of a fixed duration (Group 4). The pressure amplitudes shown in Table 1 refer to free field peak-positive pressures measured in water, and the corresponding spatial-peak temporal-peak acoustic intensities were approximated from these pressure measurements.

AO sensing sub-system

A 1064 nm CW Nd:YAG laser (IRCL-700-1064-S, CrystaLaser, CA, USA) was used as the light source for this study. The output of the laser was split into a signal beam and a reference beam by a variable beam splitter. The signal beam was expanded to a diameter of 16 mm and directed along the Y axis passing through the transparent walls of the tank and holder. This beam illuminated the front surface of the sample with a calibrated optical intensity of approximately 200 mW/cm^2 , which was one fifth of the American National Standards Institute (ANSI) clinical safety limit (American National Standards Institute 2000) for this wavelength of light. The illuminating signal beam was scattered within the sample and phased modulated by the applied HIFU field within the AO interaction region. The resulting diffuse signal beam, including both “tagged” and “untagged” portions, was collected at the distal side of the sample by a lens and directed into a GaAs photorefractive crystal (PRC)-based interferometric light detector (Lai *et al.* 2009) where it was made to interfere with the reference beam. Within this detector, which is described below, the ultrasound-induced phase modulation was converted into a light intensity modulation characterized by (a) an AC term at the ultrasound center frequency and (b) a DC “offset” that is proportional to the AO interaction strength (Murray *et al.* 2004; Blonigen *et al.* 2005; Gross *et al.* 2005). The electrical signal from the detector was preamplified (20 dB), low-pass filtered (500 kHz, model 3940, Krohn-Hite, MA, USA) to eliminate the AC component, and fed into a lock-in amplifier (LIA) (SR830, Stanford Research System, CA). The 50-Hz HIFU modulation signal served as the reference signal for the LIA. This resulted in the real-time output from the LIA being proportional to the RMS value of the DC offset signal. The LIA output was recorded on a

personal computer and served as a measure of the AO interaction strength averaged over the 30 ms integration time of the LIA.

Phase demodulation using a PRC and lock-in real-time detection of AO signal amplitude

A brief overview of the principles of PRC-based interferometry for the detection of ultrasound-induced phased modulation is presented here. Further details can be found in literature (Murray *et al.* 2004; Gross *et al.* 2005; Lai *et al.* 2009).

As shown in Figure 2(a), the signal beam emanating from the sample (E_s) is collected by a lens (L1) and directed into a $7 \times 7 \times 7 \text{ mm}^3$ photorefractive crystal (MolTech GmbH, Berlin, Germany), where it mixes with the reference beam (E_r), setting up a light interference pattern that alters the local index of refraction within the crystal. As a result, part of E_r is diffracted into the direction of the transmitted signal beam ($E_{s,t}$) in a process called two-wave mixing (TWM). The diffracted reference beam ($E_{r,d}$) and the transmitted signal beam are then collected by a second lens (L2), directed through an optical band-pass filter (BPF, FL1064-3, Thorlabs, NJ, USA) to eliminate room light, and into an avalanche photodetector (APD, APD50, Pacific Silicon Sensor, CA, USA). In addition, a 2.1 kHz, 5 kV (peak-to-peak) electric field was applied across the crystal to enhance TWM efficiency.

The diffracted reference beam, in the absence of ultrasound modulation, is an exact replica of E_s . Thus, $E_{s,t}$ and $E_{r,d}$ are perfectly in phase and interfere constructively, resulting in a maximum optical intensity voltage at the photodetector (see Figure 2b). In the presence of ultrasound modulation (Figure 2c), and assuming the duration of AO interaction is temporally short with respect to the crystal response time

(order of 10 ms), the interference pattern remains stationary, as does the diffracted reference beam. Since $E_{s,t}$ is partially phase shifted by the ultrasound, $E_{s,t}$ and $E_{r,d}$ are no longer in phase, and the interference between them results in a reduction in the light detected by the APD. During the HIFU exposure this APD voltage offset is directly associated with the changes in optical properties in the AO interaction region.

An example of an averaged AO signal waveform obtained under a relatively low focal pressure (1 MPa peak positive) in *ex-vivo* tissue is illustrated in Figure 2(d). Acquisition of this signal took approximately 20 second (1000 averages). The APD output possessed a maximum of V_0 in the absence of the HIFU field. At time t_0 the HIFU field was present in the interaction region, resulting in tagged photons and a corresponding voltage offset, V_{pp} . Subsequently, when the HIFU field was off at time $t_0 + 10$ ms, the APD output gradually returned to V_0 at a rate that was governed by the response time of the PRC crystal. This trend was repeated for each modulation cycle of HIFU field. The exposure parameters used for this example were not sufficient to lesion the tissue, which resulted in a constant value for V_{pp} . However, if the optical properties of the tissue had been affected through the formation of a lesion, the increased attenuation would reduce the number of “tagged photons” and the depth of modulation (Sakadzic and Wang 2005; Kothapalli *et al.* 2007; Lai *et al.* 2009). Therefore V_{pp} would be reduced over time, as the lesion grew in size. Since the averaged waveform in Figure 2(d) took up to 20 s to acquire, simple time averaging is not suitable for real-time monitoring. The LIA was implemented in this study to increase this speed by virtue of the reduced bandwidth afforded by lock-in detection (i.e. less noise). The LIA was set with

an integration time constant of 30 ms and a 12 dB/octave roll off. The continuous output of the LIA, denoted as $S(t)$, was proportional to the RMS of V_{pp} . This value was streamed and recorded on the personal computer at a rate of 7 Hz and displayed as a function of exposure time.

The value of AO signal amplitude varied from sample to sample (Lai *et al.* 2009), so the value of $S(t)$ of each exposure was recorded and normalized as $NS(t) = S(t) / S_0$, where S_0 was the initial value for each exposure, and it was defined in this study as the mean value of $S(t)$ measured in the time window of 2-5 s from the start of the exposure, when no lesion was formed. The change of the normalized AO signal amplitude during the exposure was then quantified as

$$\Delta S(t) = |NS(t) - 1| \times 100\% = |S(t) / S_0 - 1| \times 100\% \quad (1)$$

Passive cavitation detection (PCD)

A 7.5 MHz single element, focused transducer (140-710-S, Olympus, MA, USA, diameter 15.9 mm, focal length 57 mm), was used as a passive detector of cavitation noise (see Figure 1) and installed in the central aperture of the HIFU transducer, aligned concentrically, coaxially, and confocally with respect to the HIFU field. The acoustic signals sensed by this “passive cavitation detector” (PCD) originate from two mechanisms: (a) the scattering of the fundamental and non-linear components of the HIFU field from tissue inhomogeneities and/or bubbles and (b) the broadband acoustic emissions from bubbles (Leighton 1997). The detected signals were high-pass filtered at 5 MHz (F5081, Allen Avionics, NY, USA) in order to minimize the contributions from the HIFU fundamental and its first three harmonics. The filtered signal was then

amplified by a low noise preamplifier (40 dB, Model 5185, EG&G, MD, USA) and recorded by the oscilloscope. The oscilloscope was triggered by the function generator corresponding to the start of a HIFU burst, and the PCD traces were digitized at a rate of 25 Msample/sec with a window of length of 200 μ s (with a delay of 72 μ s to allow for time of flight of the HIFU field and any emissions from the focal region). The digitized signals were downloaded through the GPIB interface to the personal computer, at a constant rate of 7 Hz. The data transfer time ultimately limited the speed of acquisition used in this study. After the exposure, the PCD signals were processed in Matlab (McLaughlan 2008) to obtain the level of broadband acoustic emissions, which served as an indicator of inertial cavitation activity in the HIFU/PCD confocal volume.

B-Mode Imaging

A Terason 2000 diagnostic ultrasound imaging system (Terason Tech, MA, USA) was used with a 128-element, 38-mm aperture linear probe (10L5, center frequency of 7.5 MHz, transmit focal distance set at 50 mm) to image the tissue samples. The array was aligned parallel to the propagation direction of the HIFU field (X axis) and perpendicular to the light path. It was aligned such that the focal peak of the HIFU was approximately in the center of the array and 50 mm away from the transducer along the imaging acoustic axis. B-mode ultrasound images were acquired immediately before and after each HIFU exposure. The presence of boiling was identified through the appearance of hyperechogenicity in the focal region of the HIFU transducer (Rabkin *et al.* 2006).

Characterization of the lesion volume

The lesion volume was estimated for each exposure. Each sample was dissected using a skin-graft knife (SM9940, Cincinnati Surgical Company, OH, USA). They were first cut along the approximate position of the HIFU focal plane (Figure 3a) in order to identify the center of the lesion in the Y direction, and then along the XZ plane to expose the central cross-section of the lesion. A photograph of this cross-section, with a millimeter scale rule, was taken using a digital camera (M763, Kodak, NY, USA) for every lesion. Figure 3(a) shows an example photograph of a lesion cross-section produced by a 3300 W/cm^2 (free field spatial-peak temporal-peak intensity, 10 MPa peak pressure) 50 s exposure, with the HIFU propagating from left to right along the X axis. A Matlab routine was developed to identify the lesion boundary in the tissue based on an iso-intensity contour threshold method, as shown in Figure 3(b). For volume estimation, it was assumed that the lesion was axis-symmetric. This is a reasonable approximation for this study which employed relatively homogeneous tissue samples devoid of large structural defects such as blood vessels, and did not employ acoustic intensities sufficient to induce substantial cavitation activity or boiling. The lesion volume, denoted as LV , was estimated using the equation

$$LV = \sum_{i=1}^N \left\{ 1 \times \pi \times \left(\frac{W_i}{2} \right)^2 / C_p^3 \right\}, \quad (2)$$

where N is the total amount of pixels along the length of the lesion, W_i is the lesion width at acoustic position i , and C_p is the pixel calibration factor, defined as the number of pixels per mm distance in the cross-section photograph. The same procedure was performed for all lesions in the study, which could then be compared with their corresponding AO signal amplitude reduction ($\Delta S(t)$). It should be mentioned here that

this calculation of lesion volume is more representative of the true geometry than describing the lesion as a circular cylinder or perfect ellipsoid (Meaney *et al.* 1998). It should also be noted that the act of removing the sample from the tissue holder might have led to geometric deformations sufficient to modify the measured dimensions of the lesion (Zheng and Vaezy 2008).

RESULTS

Figure 4(a) shows a typical non-normalized AO signal $S(t)$, for a single 3300 W/cm² (10 MPa peak pressure) 40 s HIFU exposure in *ex-vivo* chicken breast. The figure shows that $S(t)$ increased from 0 to 29 mV in less than 1 second after the HIFU was turned on. Between 2-5 s, $S(t)$ had a mean value of $S_0 = 29.5$ mV with a standard deviation of 0.29 mV. After 8 s, $S(t)$ started to decrease and obtained a value of 14.9 mV by the end of the exposure. The gray, solid curve in Figure 4(b) shows the corresponding PCD signal which remained between 0.3-0.4 volts during the exposure, indicating that no inertial cavitation was detected during this exposure. In comparison, the black, dashed curve in Figure 4(b) shows an example of PCD broadband emission as a function of time when inertial cavitation was generated during another exposure in another tissue sample with the signal associated with cavitation beginning at approximately 27 s. Two B-mode images acquired immediately before and after the non-cavitating exposure are displayed in Figure 4(c) and (d), where the dashed box indicates the approximate position of the HIFU focus. No change in echogenicity was observed as a result of this exposure, suggesting that no boiling occurred. Figure 4(e) shows the photograph of the lesion generated from this exposure, where the HIFU propagated from left to right along the X

axis. With Eq. 2, the volume of this lesion was estimated to be 252 mm^3 . Although no evidence of this lesion was identifiable from the B-mode images, the reduction in $S(t)$ during the exposure indicates a change in the optical properties of the sample.

In order to demonstrate how the AO signal is affected by lesion size, three exposures were performed in a single tissue sample at different locations along the Z direction. Each exposure had the same peak intensity (3300 W/cm^2 , 10 MPa peak pressure) but the exposure times were 5, 30 and 40 s. Figure 5(a)-(c) shows the normalized AO amplitude, $NS(t)$, and the corresponding lesion cross-sections are displayed in Figure 5(d). For each of the exposures $NS(t)$ increased from 0 to 1 in less than 1 s after the HIFU exposure was turned on. The signal spiking observed in the initial rise of (b) and (c) was related to the bandwidth of the LIA. Between 2-5 s, $NS(t)$ had a constant value of 1.00 ± 0.03 for three exposures. For the 5 s exposure, there was no change in $NS(t)$ greater than ± 0.03 throughout the entire exposure and no lesion was present at the corresponding position in the tissue upon dissection. However, for the longer exposures, $NS(t)$ started to reduce around 5-7 s, ending at 0.45 for 30 s exposure and 0.28 for 40 s exposure (Figure 5b-c). The measured lesion volumes were 250 and 470 mm^3 , respectively (Figure 5d), suggesting that the reduction in $NS(t)$ correlates with lesion volume. In both Figure 5(b) and (c), we interpret the knee of the $NS(t)$ curves at 5-7 second to indicate the onset of lesion formation.

In order to further explore the relationship between normalized AO reduction, $\Delta S(t)$, and the corresponding lesion volume, 72 exposures were performed with fixed pressure and duration (Group 1, Table 1). A further 87 exposures were performed with varied pressures and/or durations (Group 2, Table 1) to further study how the relation

between $\Delta S(t)$ and lesion volume was affected by the exposure parameters. For each of these exposures, the PCD signals and B-mode images confirmed the absence of inertial cavitation and boiling for all exposures in the study.

Figure 6(a) shows the correlation of $\Delta S(t)$ with the measured lesion volume for Groups 1 (green stars) and 2 (red circles) as well as the least square error (LSE) power fit for all of the measurements (purple line). From the Group 1 data, it can be seen that when using the same pressure and exposure duration, the ensuing lesion volumes were broadly distributed, ranging from 0 to 205 mm³. However, despite this large distribution in lesion volume, the level of $\Delta S(t)$ nevertheless is correlated with the measured volumes. This data indicates the measured reduction in AO signal level is a much better predictor of lesion formation than the acoustic source driving parameters. The correlation between $\Delta S(t)$ and lesion volume remained consistent when different exposure parameters were employed as shown from the Group 2 data in Figure 6(a). The Group 2 data is re-plotted in Figures 6(b)-(d), with the symbols in each plot corresponding to different experimental parameters. In Figure 6(b), each symbol corresponds to a given exposure time and pressure, while in Figure 6(c) each symbol represents measurements on a different chicken breast. Finally, in Figure 6(d) the symbols indicate whether the sample is thick (> 20mm) or thin (< 20mm). Taken as a whole, Figure 6 serve to underscore the wide variety of samples tested and the fact that $S(t)$ tends to track lesion volume irrespective of exposure parameters, sample source and geometry.

In order to use AO sensing to guide HIFU therapy in real time, measurements of the instantaneous $S(t)$ were continuously streamed to the computer at a rate of 7 measurements per second. HIFU exposure was continued until $\Delta S(t)$ equaled or

exceeded the user preset threshold AO change, ΔS_p , at which point the HIFU exposure was immediately terminated. A flow chart of the exposure process is given in Figure 7. To demonstrate the efficacy of this approach compared with exposures employing fixed time durations, 157 repeat exposures (Group 3, Table 1) were performed at the same peak intensity (3300 W/cm², 10 MPa peak pressure), with the exposure duration regulated in real time by the method described above. These were compared with another series of 189 exposures at a fixed intensity (Group 4, Table 1) but a number of preset exposure durations. Table 2 shows the mean and standard deviation of the resulting exposure duration corresponding to each ΔS_p for Group 3, and Figure 8 illustrates the distribution of the resulting lesion volumes as a function of (mean) exposure durations for Groups 3 and 4. As we can see from Figure 8, when the exposure durations and/or the mean of lesion volumes were approximately equivalent, a 30-40% decrease in the standard deviation of the lesion volumes was obtained when a preset AO reduction threshold was used as the criteria to guide the exposures. In addition, the lesion volumes shown in Figure 8 for different ΔS_p agree quite well with the estimated lesion volumes based on the LSE fit in Figure 6(a).

DISCUSSION

AO monitoring of exposures

The objective of this study was to develop an integrated AO sensing system to monitor the onset and growth of HIFU lesions in *ex-vivo* chicken breast in real time. The amplitude of the detected AO signal is affected by a number of parameters which

included the amount of light reaching the AO interaction region, the optical path length through the tissue, the characteristics of the ultrasound field, the characteristics of the PRC configuration (size, absorption coefficient and TWM gain coefficient), as well as the optical properties of the AO interaction region (Lai *et al.* 2009). In Figure 4(a), $S(t)$ displays a sharp increase coincident with the onset of HIFU exposure, for AO interaction can occur only when both light and sound coexist. The AO signal then remained constant until a lesion formed at which point there was a gradual reduction in the AO signal caused by an increase in the optical absorption and scattering coefficients associated with the formation of a lesion within the AO interaction region. The existence of the lesion was confirmed by the cross-sectional photograph (Figure 4d). We note that lesions created in this study did not yield detectable cavitation activity during exposure, nor could they be visualized post-exposure with B-mode ultrasound due to the absence of boiling bubbles. These data suggest that AOI offers more robust detection of non-cavitating lesions than B-mode ultrasound.

It was found (Figure 5a-d) that the AO response was correlated with the lesion volume. The extent of the lesion depends on a number of factors, such as the profile and the intensity of the HIFU field, exposure duration, acoustic path length in the tissue, as well as the physical properties and the functional status of the overlying tissues between the transducer and the focal region (ter Haar 1995; Meaney *et al.* 1998; Wang *et al.* 2003). Samples that were found to contain large blood vessels upon subsequent dissection photography were excluded from the data set in this study. Despite constant HIFU pressure and exposure duration, large variations in the ensuing lesion volumes were observed (Figure 6a, Group 1), likely due to inhomogeneities in the tissue samples, which

can cause acoustic reflection, refraction, scattering and diffraction (Wang *et al.* 2003). The large variations in lesion volumes were in agreement with previously published data (ter Haar *et al.* 1989; Meaney *et al.* 1998; Wang *et al.* 2003; Li *et al.* 2006).

A key finding in this study is that the change in the normalized AO signal amplitude during an exposure was proportional to the volume of the resultant lesion (Figure 6a-d), and the correlation was unaffected by the exposure parameters, sample source and sample geometry at the given range. This is the case because the normalized AO amplitude reduction, as discussed earlier, was solely a result of the formation of a lesion. The larger the volume of such a lesion, the fewer the number of photons “tagged” by the ultrasound, resulting in a greater reduction in AO. Therefore, the change in AO response during exposure can potentially be used to determine the onset and development of a HIFU lesion. This is of significance since real-time feedback of lesion formation is still a challenge for HIFU treatments.

AO-guided exposures

To guarantee the efficacy of HIFU treatments it is important to ensure that the desired tumor volume is necrosed while damage to neighboring healthy tissues is kept to a minimum. Therefore, the ability to predict the size and shape of necrosed regions is of importance. Unfortunately, the volumes of individual lesions, many of which would be required to ablate a complete tumor, can vary due to the aforementioned factors. As a result, inadequate or excessive heating might be employed in practice, resulting in incomplete tumor ablation or damage of healthy tissues. In this study, the use of AO sensing was proposed as an exposure-guidance method in order to obtain less variability

in lesion volume (Figure 7). Statistical analysis of the measurements (Figure 8) demonstrated significant improvements in the consistency and repeatability of individual lesion volumes by using feedback from AO sensing in contrast with using fixed exposure parameters to guide tissue necrosis. It should be mentioned at this point that these measurements were performed in relatively homogeneous chicken breast samples, representing the best scenario for HIFU exposures. For *in vivo* applications, exposures with fixed duration would produce more diverse lesions in terms of volume, whereas the AOI-guided exposures should be immune to such changes as the AO response is normalized to the initial level for each exposure. These suggest that AO sensing could potentially be used to improve treatment planning and efficacy evaluation.

Limitations of lesion detection

In our experimental setup, accurate prediction of lesion volume was limited by the size of the HIFU focal volume, which consequently limits the AO sensing volume. (AO signal strength is roughly quadratic in the pressure amplitude (Lai *et al.* 2009).) This effect was reflected in the correlation curve in Figure 6. When the lesion volume was less than 40 mm^3 (corresponding to the contour volume of FWHM of the peak pressure), $\Delta S(t)$ increased approximately linearly with the lesion volume, as expected. Above 40 mm^3 , however, the curve plateaued due to the pressure contours of the HIFU field, outside of the main focal zone, giving a lower detection sensitivity for AO. In order to accurately detect or guide the formation of larger lesions, the AO sensing region could be expanded by using an additional transducer with a larger focal field to pump the AO interaction, provided this larger beam does not exceed the optical illumination region.

Improvement of effective detection depth

The most critical limitation of this system comes from the limited detection depth in tissue caused by the typically low SNR of AO signals. Presently, the majority of AO systems (Murray *et al.* 2004; Ramaz *et al.* 2004; Sakadzic and Wang 2004; Bossy *et al.* 2005; Kim *et al.* 2006; Bossy *et al.* 2007; Li *et al.* 2008; Lai *et al.* 2009), including the one used in this study, employ CW lasers as the light sources, where the maximum permissible clinical exposure is strictly limited (American National Standards Institute 2000). In addition, only the light traversing the AO interaction region is modulated by the ultrasound, which is typically detected against a much stronger background of unmodulated light. The total amount of tagged light that can be collected outside the tissue sample is therefore small and the SNR is poor. The *ex-vivo* tissue sample thickness in this study (less than 30 mm) did not test the upper limit of system sensitivity. However, the system described in this paper was not optimized for clinical applications where desired depths are typically more than 50 mm (Wang 1998). Given recent progress in increasing signal SNR by using a pulsed laser with high peak intensity but low duty cycle (Rousseau *et al.* 2008) and/or the possibility of more efficient demodulators based, for example, on spectral-hole burning crystals (SHBC) (Li *et al.* 2008), it is likely that deeper and faster detection using AO interactions will become a reality. Thus, this technique could be extended to *in vivo* HIFU applications in optically accessible tissues such as breast, brain and prostate.

Optical illumination and detection alignment

The AO system described in this study employs a transillumination geometry, where the laser source and detector are on the opposite sides of the sample, with the ultrasound propagating perpendicular to the source and detector. This alignment, however, is a drawback for medical imaging, as in many cases transillumination is impracticable or leads to much larger penetration depth. A more convenient configuration is to install the source and detector on the same surface of the sample as in traditional optical spectroscopy techniques. The feasibility of this reflection configuration for AO imaging has been successfully demonstrated (Lev *et al.* 2000; Granot *et al.* 2001; Li and Wang 2004; Sakadzic and Wang 2004; Kothapalli and Wang 2009). However, it should be noted that the background (“untagged”) photon flux is higher in a reflection geometry than in a transillumination geometry, which makes detection of the tagged photons emanating from deep within the tissue more challenging.

Real-time imaging of lesion formation

In this study, the AO amplitude change, monitored in real time, was used as a metric to infer the size of the lesion formed in the tissue sample. However, with potential improvements in system SNR such as those discussed above, real-time 2-D imaging of the HIFU focal region during the exposure may be feasible. This could be accomplished by using a clinical ultrasound-imaging machine to both form B-mode structural images *and* pump the AO response. This approach was used for imaging optical absorption contrast by Bossy *et al.* (2005) in tissue phantoms and excised tissue samples.

CONCLUSIONS

In this study, a photorefractive crystal based AO sensing system operating in the near-infrared optical wavelength was described and used to sense and monitor, in real time, the formation of lesions under HIFU exposure. The same HIFU field induced tissue heating and pumped the AO interaction. Because the same acoustic beam was used for both therapy and sensing, alignment was automatic. The AO signal amplitude change during an exposure was correlated with the resulting lesion volume, which suggests that AO sensing could improve the efficacy of HIFU exposure evaluation in organs that support diffusive optical fields; notably breast, brain, and prostate. The use of AO sensing for real-time feedback yielded a 30-40% improvement in the consistency of the resultant lesion volumes compared with fixed duration exposures. Although the system was not optimized for *in vivo* trials, this exploratory study indicates that *in vivo* HIFU guidance using AO sensing may indeed be feasible. Moreover the technique studied in this paper is not limited to HIFU therapy, but could potentially be used for treatment monitoring of other thermal ablation therapies such as laser and microwave.

Acknowledgement- The authors acknowledge the financial support of the Bernard M. Gordon Center for Subsurface Sensing and Imaging Systems under the Engineering Research Centers Program of the National Science Foundation (Award number EEC-9986821). We thank Dr. A. P. Evan of the Indiana University School of Medicine for use of the fiber-optic hydrophone.

REFERENCES

American National Standards Institute. American National Standard for the Safe Use of Laser in Health Care Facilities, ANSI Z136.1. American National Standards Institute, New York, 2000.

Bailey MR, Couret LN, Sapozhniko OA, Khokhlova BA, ter Haar GR, Vaezy S, Shi X, Martin R, Crum LA. Use of overpressure to assess the role of bubbles in focused ultrasound lesion shape in vitro. *Ultrasound Med Biol* 2001;27:695-708.

Ben-David M, Cantor R, Balbul N, Yehuda M, Gannot I. Measuring tissue heat penetration by scattered light measurements. *Lasers in Surgery and Medicine* 2008;40:494-9.

Black JF, Barton JK. Chemical and structural changes in blood undergoing laser photocoagulation. *Photochem Photobiol* 2004;80:89-97.

Blonigen FJ, Nieva A, DiMarzio CA, Manneville S, Sui L, Maguluri G, Murray TW, Roy RA. Computations of the acoustically induced phase shifts of optical paths in acoustophotonic imaging with photorefractive-based detection. *Appl Opt* 2005;44:3735-46.

Boas DA, Brooks DH, Miller EL, Dimarzio CA, Kilmer M, Gaudette RJ, Zhang Q. Imaging the body with diffuse optical tomography. *IEEE Signal Processing Magazine* 2001;18:57-75.

Bossy E, Sui L, Murray TW, Roy RA. Fusion of conventional ultrasound imaging and acousto-optic sensing by use of a standard pulsed-ultrasound scanner. *Opt Lett* 2005;30:744-6.

Bossy E, Funke AR, Daoudi K, Boccara AC. Transient optoelastography in optically diffusive media. *Appl Phys Lett* 2007;90:174111.

Chan AH, Fujimoto VY, Moore DE, Martin RW, Vaezy S. An image-guided high intensity focused ultrasound device for uterine fibroids treatment. *Med Phys* 2002;29:2611-20.

Cilesiz IF, Welch AJ. Light dosimetry: effects of dehydration and thermal damage on the optical properties of the human aorta. *Appl Opt* 1993;32:477-87.

Cline HE, Schenck JF, Watkins RD, Hynynen K, Jolesz FA. Magnetic resonance-guided thermal surgery. *Magn Reson Med* 1993;30:98-106.

Coussios C, Farny CH, Haar GT, Roy RA. Role of acoustic cavitation in the delivery and monitoring of cancer treatment by high-intensity focused ultrasound (HIFU). *Int J Hyperthermia* 2007;23:105-20.

Dolfi D and Micheron F. Imaging process and system for transillumination with photon frequency marking. International Patent 1989; WO 89/00278.

Furusawa H, Namba K, Thomsen S, Akiyama F, Bendet A, Tanaka C, Yasuda Y, Nakahara H. Magnetic resonance-guided focused ultrasound surgery of breast cancer: reliability and effectiveness. *J Am Coll Surg* 2006;203:54-63.

Gelet A, Chapelon JY, Bouvier R, Rouviere O, Lasne Y, Lyonnet D, Dubernard JM. Transrectal high-intensity focused ultrasound: minimally invasive therapy of localized prostate cancer. *J Endourol* 2000;14:519-28.

Gianfelice D, Amara M, Belblidia A, Boulanger Y. MR Imaging-guided Focused US Ablation of Breast Cancer: Histopathologic Assessment of Effectiveness—Initial Experience. *Radiology* 2003a;227:849-55.

Gianfelice D, Khiat A, Boulanger Y, Amara M, Belblidia A. Feasibility of magnetic resonance imaging-guided focused ultrasound surgery as an adjunct to tamoxifen therapy in high-risk surgical patients with breast carcinoma. *J Vasc Interv Radiol* 2003b;14:1275-82.

Granot E, Lev A, Kotler Z, Sfez BG. Detection of inhomogeneities with ultrasound tagging of light. *J Opt Soc Am A* 2001;18:1962-7.

Gross M, Ramaz F, Forget BC, Atlan M, Boccara AC, Delaye P, Roosen G. Theoretical description of the photorefractive detection of the ultrasound modulated photons in scattering media. *Opt Express* 2005;13:7097-112.

Hill CR, ter Haar GR. High intensity focused ultrasound- potential for cancer treatment (Review article). *Br J Radiol* 1995;68:1296-303.

Hynynen K, Freund WR, Cline HE, H. CA, Watkins RD, Vetro JP, Jolesz FA. A clinical, noninvasive, MR imaging-monitored ultrasound surgery method. *Radiographics* 1996;16:185-95.

Illing R, Chapman A. The clinical applications of high intensity focused ultrasound in the prostate. *Int J Hyperthermia* 2007;23:183-91.

Kennedy JE, Wu F, ter Haar GR, Gleeson FV, Phillips RR, Middleton MR, Cranston D. High-intensity focused ultrasound for the treatment of liver tumors. *Ultrasonics* 2004;42:931-5.

Kennedy JE. High-intensity focused ultrasound in the treatment of solid tumours. *Nat Rev Cancer* 2005;5:321-7.

Khokhlova TD, Pelivanov IM, Sapozhniko OA, Solomatin VS, Karabutov AA. Opto-acoustic diagnostics of the thermal action of high-intensity focused ultrasound on

biological tissues: the possibility of its applications and model experiments. *Quantum Electronics* 2006;36:1097-102.

Khokhlova TD, Canney MS, Lee D, Marro KI, Crum LA, Khokhlova VA, Bailey MR. Magnetic resonance imaging of boiling induced by high intensity focused ultrasound. *J Acoust Soc AM* 2009;125:2420-31.

Kim C, Zemp RJ, Wang LV. Intense acoustic bursts as a signal-enhancement mechanism in ultrasound-modulated optical tomography. *Opt Lett* 2006;31:2423-5.

Kohrman KU, Michel MS, Gaa J, Marlinghaus E, Alken P. High intensify focused ultrasound as noninvasive therapy for mutilocal renal cell carcinoma: case study and review of the literature. *J Urol* 2002;167:2397-403.

Konofagou EE, Thierman J, Hynynen K. The use of ultrasound-stimulated acoustic emission in the monitoring of modulus changes with temperature. *Ultrasonics* 2003;41:337-45.

Kopelman D, Inbar Y, Hanannel A, Freundlich D, Castel D, Perel A, Greenfeld A, Salamon T, Sareli M, Valeanu A, Papa M. Magnetic resonance-guided focused ultrasound surgery (MRgFUS): Ablation of liver tissue in a porcine model. *European Journal of Radiology* 2006;59:157-62.

Kothapalli S-R, Sakadzic S, Kim C, Wang LV. Imaging optically scattering objects with ultrasound-modulated optical tomography. *Opt Lett* 2007;32:2351-3.

Kothapalli S-R, Wang L. Ex vivo blood vessel imaging using ultrasound-modulated optical microscopy. *Journal of Biomedical Optics* 2009;14:014015-1.

Lai P, Roy RA, Murray TW. Quantitative characterization of turbid medium using pressure contrast acousto-optic imaging. *Optics Letters* 2009;34:2850-2.

- Leighton TG. The Acoustic Bubble. San Diego, CA: Academic Press, Inc., 1997.
- Leutz W, Maret G. Ultrasonic modulation of multiply scattered light. *Physica B* 1995;204:14-9.
- Lev A, Kotler Z, Sfez BG. Ultrasound tagged light imaging in turbid media in a reflectance geometry. *Opt Lett* 2000;25:378-80.
- Lewa CJ. Magnetic-resonance-imaging in the presence of mechanical waves. *Spectrosc Lett* 1991;24:55-67.
- Li F, Feng R, Zhang Q, Bai J, Wang Z. Estimation of HIFU induced lesions in vitro: numerical simulation and experiment. *Ultrasonics* 2006;44:e337-e40.
- Li J, Wang LV. Ultrasound-modulated optical computed tomography of biological tissues. *Appl Phys Lett* 2004;84:1597-9.
- Li Y, Hemmer P, Kim C, Zhang H, Wang LV. Detection of ultrasound-modulated diffuse photons using spectral hole burning. *Optics Express* 2008;16:14862-74.
- Lizzi FL, Muratore R, Deng CX, Kettering JA, Alam SK, S. M, Kalisz A. Radiation-force technique to monitor lesions during ultrasonic therapy. *Ultrasound Med Biol* 2003;29:1593-605.
- Maleke C, Konofagou EE. Harmonic motion imaging for focused ultrasound (HMOFU): a fully integrated technique for sonication and monitoring of thermal ablation in tissues. *Phys Med Biol* 2008;53:1773-93.
- Marks FA, Tomlinson HW, Brooksby GW. A comprehensive approach to breast cancer detection using light: photon localization by ultrasound modulation and tissue characterization by spectral discrimination. *SPIE* 1993;1888:500-10.

McDannold N, Hynynen K, Wolf D, Wolf G, Jolesz FA. MRI evaluation of thermal ablation of tumors with focused ultrasound. *J Magn Reson Imaging* 1998;8:91-100.

McLaughlan JR. An investigation into the use of cavitation for the optimisation of high intensity focused ultrasound (HIFU) treatments. Doctor of Philosophy in Physics, 2008. London: University of London, Joint Department of Physics, Institute of Cancer Research and Royal Marsden NHS Trust.

Meaney PM, Clarke RL, ter Haar GR, Rivens IH. A 3-D finite-element model for computation of temperature profiles and regions of thermal damage during focused ultrasound surgery exposures. *Ultrasound Med Biol* 1998;24:1489-99.

Meaney PM, Cahill MD, ter Haar GR. The intensity dependence of lesion position shift during focused ultrasound surgery. *Ultrasound Med Biol* 2000;26:441-50.

Murray TW, Sui L, Maguluri G, Roy RA, Nieva A, Blonigen FJ, DiMarzio CA. Detection of ultrasound-modulated photons in diffuse media using the photorefractive effect. *Opt Lett* 2004;29:2509-11.

Murray TW, Roy RA. Illuminating Sound: Imaging Tissue Optical Properties with Ultrasound. *Acoustics Today* 2007;3:17-23.

Ng KY, Liu Y. Therapeutic ultrasound: its application in drug delivery. *Med Res Rev* 2002;22:204-23.

Nilsson AMK, Stureson C, Liu DL, Andersson-Engels S. Changes in spectral shape of tissue optical properties in conjunction with laser-induced thermotherapy. *Appl Opt* 1998;37:1256-67.

Porter TR, Xie F. Therapeutic ultrasound for gene delivery. *Echocardiography* 2001;18:349-53.

Quaresima V, Matcher SJ, Ferrari M. Identification and quantification of intrinsic optical contrast for near-infrared mammography. *Photochem Photobiol* 1998;67:4-14.

Rabkin BA, Zderic V, Vaezy S. Hyperecho in ultrasound images of HIFU therapy: involvement of cavitation. *Ultrasound Med Biol* 2005;31:947-56.

Rabkin BA, Zderic V, Crum LA, Vaezy S. Biological and physical mechanisms of HIFU-induced hyperecho in ultrasound image. *Ultrasound Med Biol* 2006;32:1721-9.

Ramaz F, Forget BC, Atlan M, Boccara AC. Photorefractive detection of tagged photons in ultrasound modulated optical tomography of thick biological tissues. *Opt Express* 2004;12:5469-74.

Rivens I, Shaw A, Civale J, Morris H. Treatment monitoring and thermometry for therapeutic focused ultrasound. *Int J Hyperthermia* 2007;23:121-39.

Rosenschein U, Furman V, Kerner E, Fabian I, Bernheim J, Eshel Y. Ultrasound Imaging–Guided Noninvasive Ultrasound Thrombolysis : Preclinical Results. *Circulation* 2000;102:238-45.

Rousseau G, Blouin A, Monchalain J-P. Ultrasound-modulated optical imaging using a powerful long pulse laser. *Opt Express* 2008;16:12577-90.

Sakadzic S, Wang LV. High resolution ultrasound-modulated optical tomography in biological tissues. *Opt Lett* 2004;29:2770-2.

Sakadzic S, Wang LV. Modulation of multiply scattered coherent light by ultrasound pulses: An analytical model. *Phys Rev E* 2005;72:033620.

Solymar L, Webb DJ, Jepsen AG. *The Physics and Applications of Photorefractive Materials*. Oxford: Clarendon Press, 1996.

Stewart EA, Gedroyc WMW, Tempany CMC, Quade BJ, Inbar Y, Ehrenstein T, Shushan A, Hindley JT, Goldin RD, David M, Sklair M, Rabinovici J. Focused ultrasound treatment of uterine fibroid tumors: Safety and feasibility of a noninvasive thermoablative technique *Am J Obstet Gynecol* 2003;189:48-54.

Sui L, Roy RA, Dimarzio CA, Murray TW. Imaging in diffuse media with pulsed-ultrasound-modulated light and the photorefractive effect. *Appl Opt* 2005;44:4041-8.

Tempany CM, Stewart EA, McDannold N, Quade BJ, Jolesz FA, Hynynen K. MR imaging-guided focused ultrasound surgery of uterine leiomyomas: A feasibility study. *Radiology* 2003;226:897-905.

ter Haar GR, Sinnett D, Rivens I. High intensity focused ultrasound - a surgical technique for treatment of discrete liver tumors. *Phys Med Biol* 1989;34:1743-50.

ter Haar GR. Ultrasound focal beam surgery. *Ultrasound Med Biol* 1995;21:1089-100.

Thuroff S, Chaussy C, Vallancien G, Wieland W, Kiel H, le Duc A, Desgrandchamps F, de la Rosette JJMCH, Gelet A. High-Intensity Focused Ultrasound and Localized Prostate Cancer: Efficacy Results from the European Multicentric Study. *J Endourol* 2003;17:673-7.

Uchida T, Sanghvi NT, Gardner TA, Koch MD, Ishii D, Minei S, Satoh T, Hyodo T, Irie A, Baba S. Transrectal high-intensity focused ultrasound for treatment of patients with stage T1b-2n0m0 localized prostate cancer: a preliminary report. *Urology* 2002;59:394-8.

Vaezy S, Martin R, Yaziji H, Kaczkowski P, Keilman G, Carter S, Caps M, Chi E, Bailey MR, Crum LA. Hemostasis of punctured blood vessels using high-intensity focused ultrasound. *Ultrasound Med Biol* 1998;24:903-10.

Vaezy S, Shi X, Martin EC, Nelson NI, Bailey MR, Crum LA. Real-time visualization of high-intensity focused ultrasound treatment using ultrasound imaging. *Ultrasound Med Biol* 2001;27:33-42.

Vallancien G, Chartier-Kastler E, Harouni M. Focused extracorporeal pyrotherapy: experimental study and feasibility in man. *Semin Urol* 1993;11:7-9.

Wang LV, Jacques SL, Zhao X. Continuous-wave ultrasonic modulation of scattered laser light to image objects in turbid media. *Opt Lett* 1995;20:629-31.

Wang LV. Ultrasonic modulation of scattered in turbid media and a potential novel tomography in biomedicine. *Photochem Photobiol* 1998;67:41-9.

Wang LV. Mechanisms of ultrasound modulation of multiply scattered coherent light: An analytic model. *Phys Rev Lett* 2001;87:043903.

Wang W, Wang Y, Tang J. Safety and efficacy of high intensity focused ultrasound ablation therapy for adenomyosis. *Acad Radiol* 2009;16:1416-23.

Wang Z, Bai J, Li F, Du Y, Wen S, Hu K, Xu G, Ma P, Yin N, Chen W, Wu F, Feng R. Study of a "biological focal region" of high-intensity focused ultrasound. *Ultrasound Med Biol* 2003;29:749-54.

Wu F, Wang Z, Cao Y, Chen W, Bai J, Zou J, Zhu H. A randomized clinical trial of high-intensity focused ultrasound ablation for the treatment of patients with localized breast cancer. *Br J Cancer* 2003a;89:2227-33.

Wu F, Wang Z, Chen W, Bai J, Zhu H, Qiao T. Preliminary experience using high-intensity focused ultrasound for the treatment of patients with advanced stage renal malignancy. *J Urol* 2003b;170:2237-40.

Wu F, Wang Z, Chen W, Zou J, Bai J, Zhu H, Li K, Xie F, Jin C, Su H, Gao G. Extracorporeal focused ultrasound surgery for treatment of human solid carcinomas: early Chinese clinical experience *Ultrasound Med Biol* 2004;30:245-60.

Wu F, Wang Z, Zhu H. Feasibility of US-guided high-intensity focused ultrasound treatment in patients with advanced pancreatic cancer: initial experience. *Radiology* 2005;236:1034-40.

Xie B, Ling J, Zhang W, Huang X, Zhen J, Huang Y. The efficacy of high-intensity focused ultrasound (HIFU) in advanced pancreatic cancer. *Clin Oncol Cancer Res* 2008;5:183-6.

Yaroslavsky AN, Schulze PC, Yaroslavsky IV, Schober R, Ulrich F, Schwartz H-J. Optical properties of selected native and coagulated human brain tissues in vitro in the visible and near infrared spectral range. *Phys Med Biol* 2002;47:2059-73.

Zheng X, Vaezy S. A localization methods of lesions induced by high intensity focused ultrasound based on acoustic backscatter change. 30th Annual International IEEE EMBS Conference 2008;3673-6.

FIGURE CAPTIONS

Figure 1. A schematic representation of the experimental setup used in this study. In this depiction, Z is the downward vertical direction. There are individual subsystems for (1) generation of the HIFU field, (2) generation of the optical field, (3) detection of acousto-optic signal, (4) passive detection of cavitation noise during exposure, and (5) post-exposure detection of boiling lesions via B-mode ultrasound imaging.

Figure 2. A schematic of the optical detection system (a) and the principle of photorefractive two-wave-mixing (TWM) effect in the absence (b) and the presence (c) of ultrasound modulation. E_s is the scattered signal beam collected from the diffuse sample, E_r is the reference beam, $E_{s,t}$ and $E_{r,t}$ are the transmitted signal and reference beams through the PRC, respectively, and $E_{r,d}$ is the reference beam energy diffracted into the direction of signal beam. (d) A typical time domain AO signal monitored at the output of the active low-pass filter (see Fig. 1) using a relatively low ultrasound focal pressure (1 MPa peak positive) in *ex-vivo* chicken breast. This waveform was obtained by coherently averaging over 1,000 sweeps (10-ms HIFU bursts), which took more than 20 s.

Figure 3. (a) Cross-section photo of a lesion produced in *ex-vivo* chicken breast by a 3300 W/cm² (spatial-peak, temporal-peak intensity, 10 MPa peak pressure) 50 s exposure. The

HIFU direction was from left to right, with its focal plane positioned 16 mm into the tissue. (b) Photograph of the lesion with its boundary delineated by dashed black lines.

Figure 4. Examples for a typical 3300 W/cm^2 (peak intensity, 10 MPa peak pressure) 40 s exposure in *ex-vivo* chicken breast: (a) non-normalized AO signal amplitude as a function of exposure time; (b) PCD signal as a function of time (gray, solid curve) corresponding to this exposure indicating no inertial cavitation, which is compared with an example (black, dashed curve) with the presence of inertial cavitation during the exposure; B-mode ultrasound images acquired immediately before (c) and after (d) the exposure (the dashed box indicates the approximate location of the HIFU focus); (e) photograph of the cross-section of the lesion generated by this exposure (HIFU field propagated from left to right, and the bar length represents 5 mm spatially).

Figure 5. Normalized AO signal amplitude as a function of time for three HIFU exposures in one single tissue sample with the same peak intensity (3300 W/cm^2 , 10 MPa peak pressure) but different durations: (a) 5 s; (b) 30 s; and (c) 40 s. (d) Photographs of the generated lesions.

Figure 6. (a) The normalized AO signal amplitude change ΔS as a function of resulting lesion volume for Group 1 (stars) and Group 2 (circles) exposures as well as the LSE fit for the data (line). The relationship between ΔS and lesion volume for Group 2

exposures are categorized according to the (b) exposure parameters (c) tissue sample, where each color symbol represents one sample cut from the same chicken breast, and (d) sample thickness.

Figure 7. The feedback method used for guiding the HIFU exposure using the measured AO response.

Figure 8. Lesion volume as a function of exposure duration for exposures guided by AO response (red, blank columns, with 20, 30, 40, 50 and 60% preset ΔS_p from left to right) and exposures with fixed durations (green, filled columns, with 25, 30, 40, 50, 60, and 75 s from left to right). The height of the column and the error bar represent the mean value and the standard deviation of the lesion volumes, respectively.

TABLES

Table 1 HIFU exposure parameters. The peak pressures were measured in water and the intensities estimated by the equation $I = P_k^2 / (2\rho c)$, where P_k is the peak positive pressure in water; ρ is the mass density of water, 1000 kg/m³; and c is the sound speed in water, 1500 m/s. Durations are not reported for Group 3 as they were determined by changes in the AO response.

	Duration (s)	Peak pressure (MPa)	Peak intensity (W/cm ²)	Number of exposures
Group 1	40	8	2100	72
Group 2	5-60	6-10	1200-3300	87
Group 3	N/A	10	3300	157
Group 4	25-75	10	3300	189

Table 2 Mean and standard deviation of durations for Group 3 exposures

ΔS_p (%)	20	30	40	50	60
Mean (s)	25	31	38	57	67
Standard deviation (s)	7	9	10	15	22

Figure 1
[Click here to download high resolution image](#)

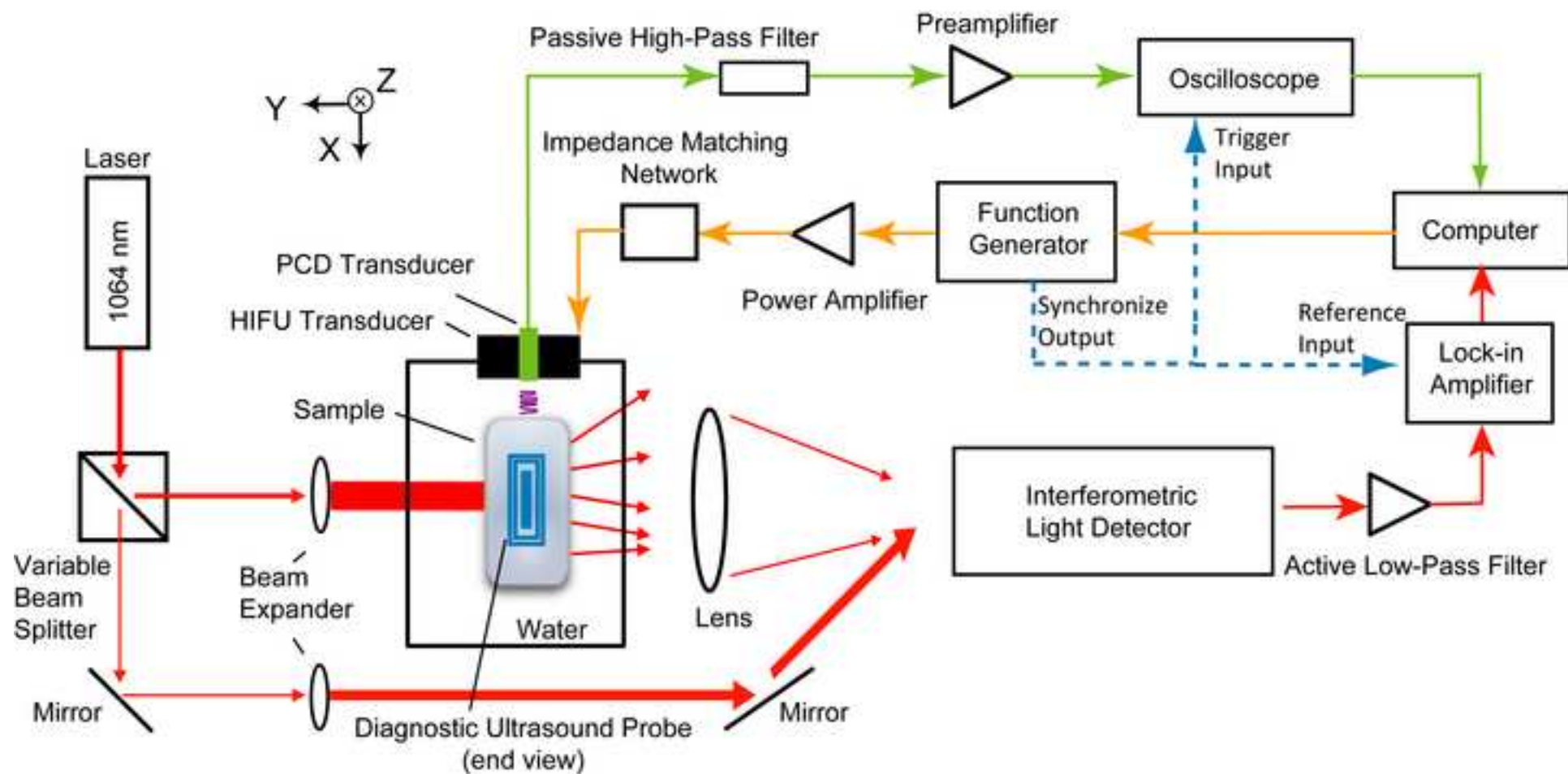


Figure 2
[Click here to download high resolution image](#)

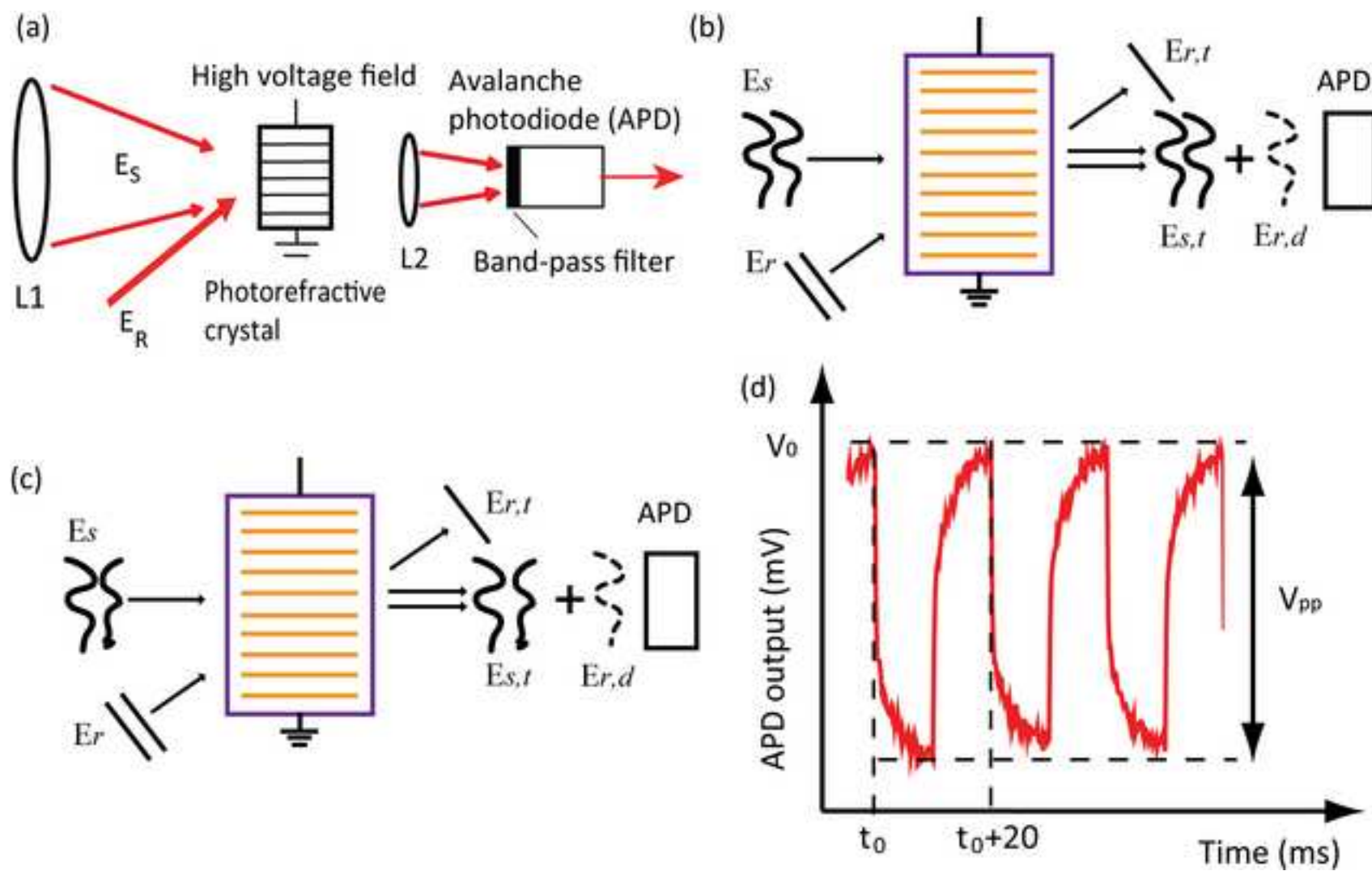


Figure 3
[Click here to download high resolution image](#)

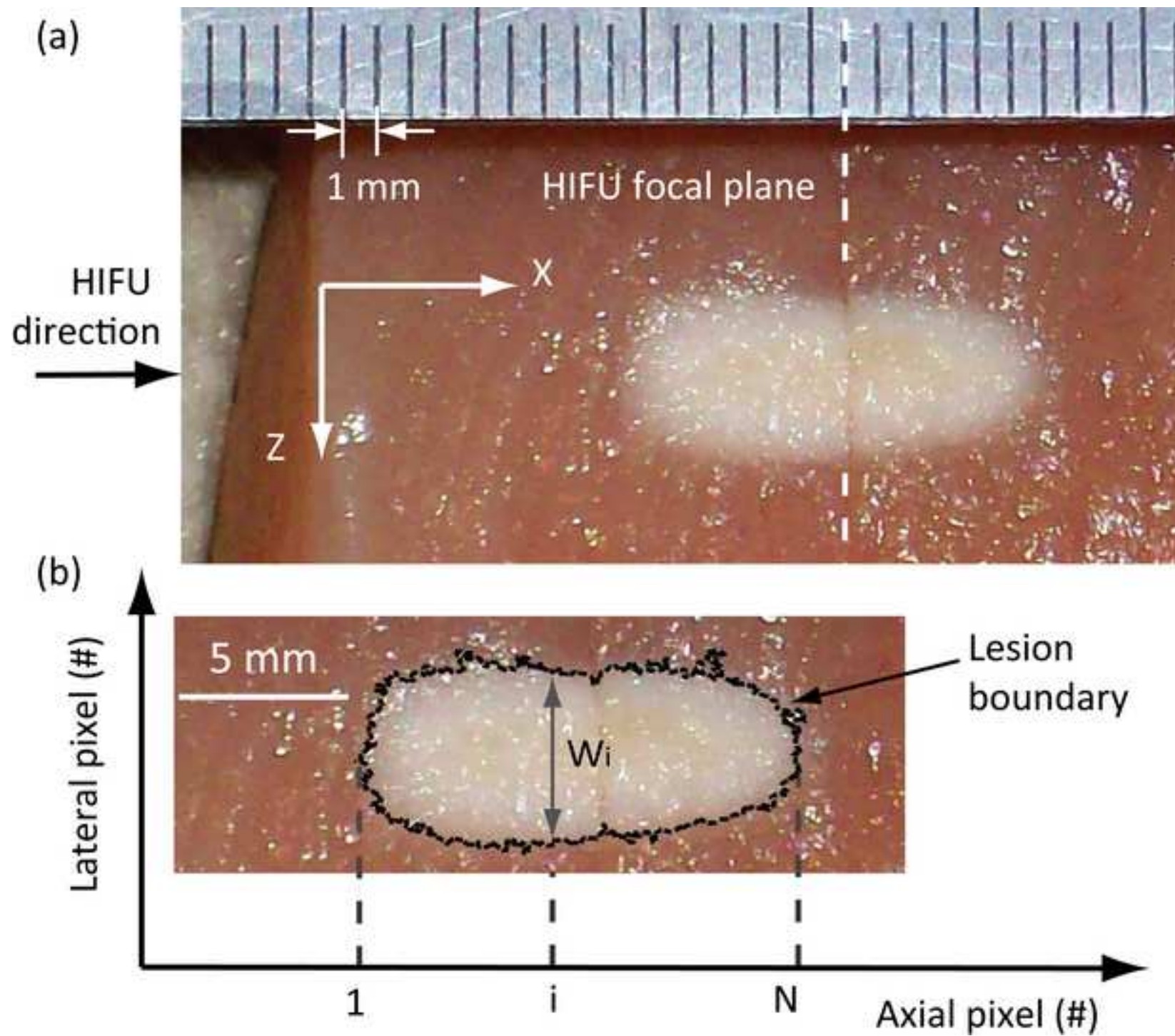


Figure 4
[Click here to download high resolution image](#)

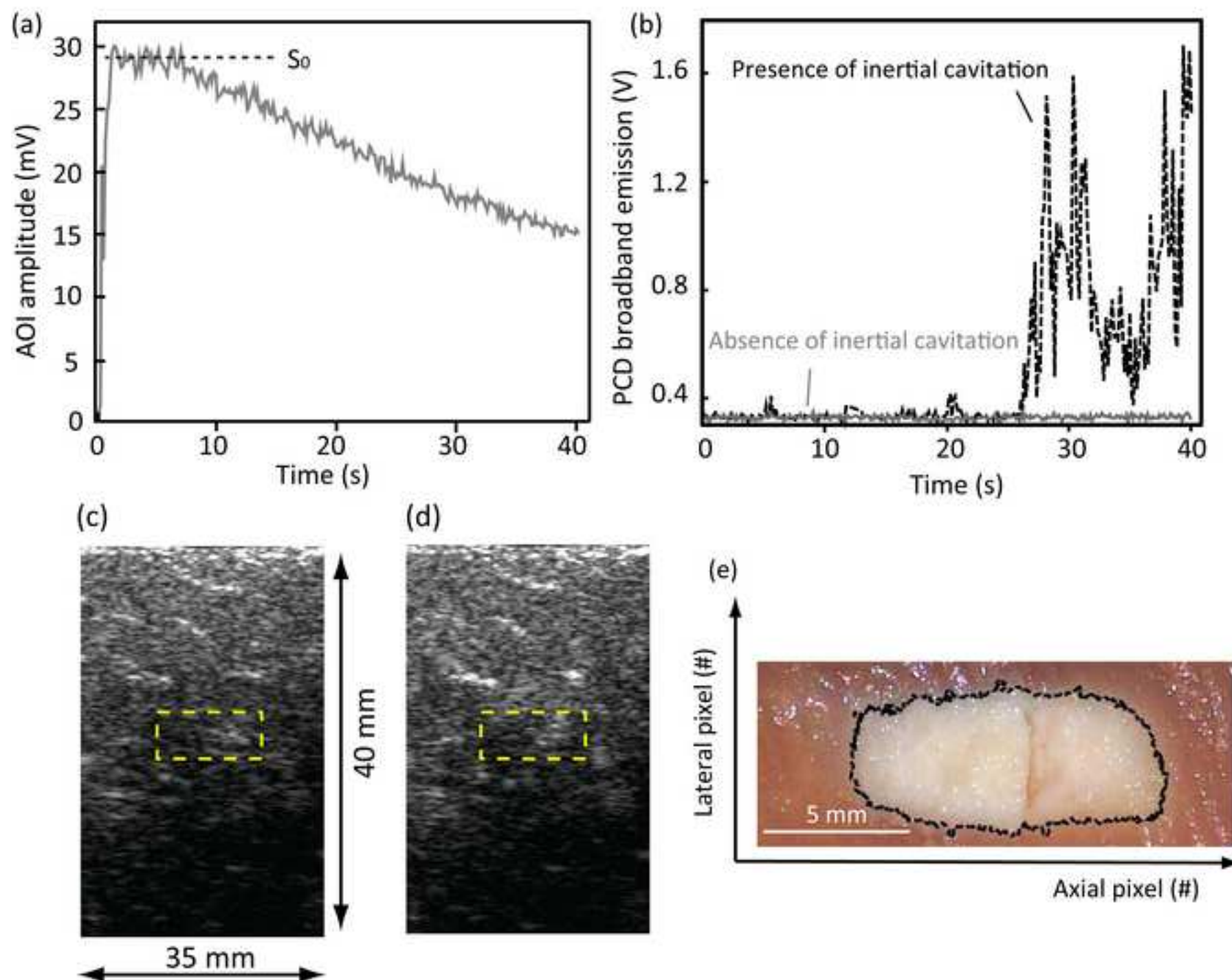


Figure 5
[Click here to download high resolution image](#)

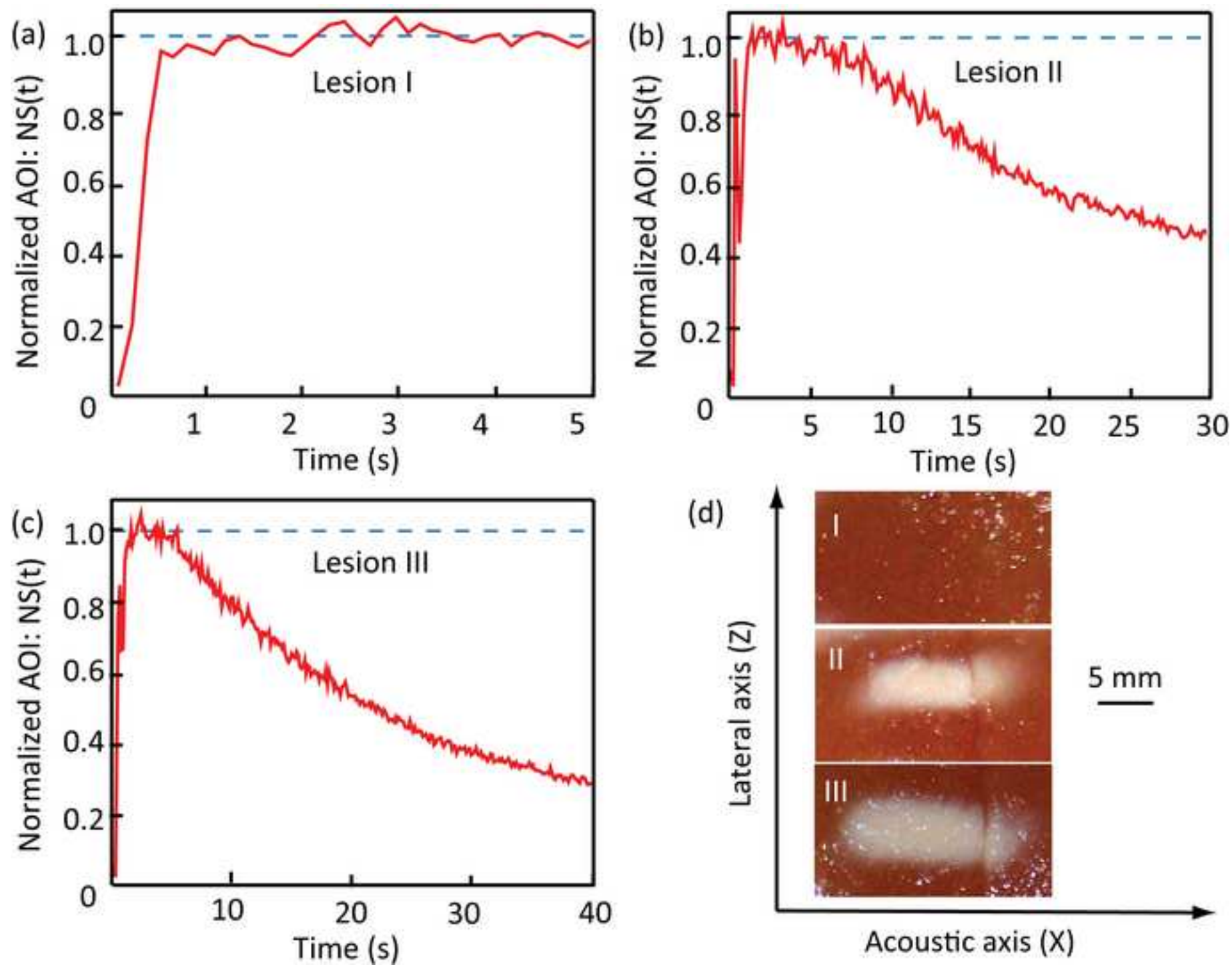


Figure 6
[Click here to download high resolution image](#)

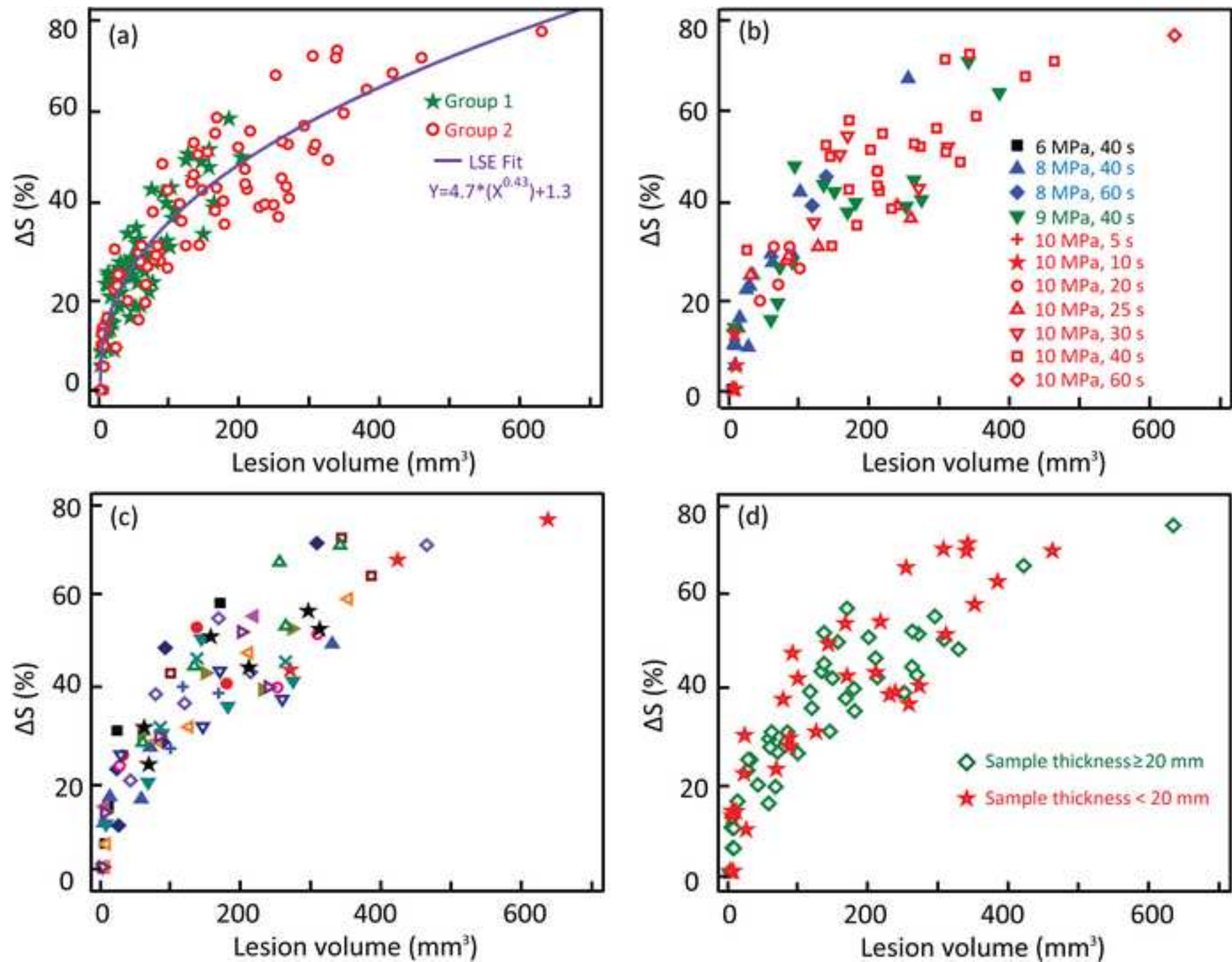


Figure 7
[Click here to download high resolution image](#)

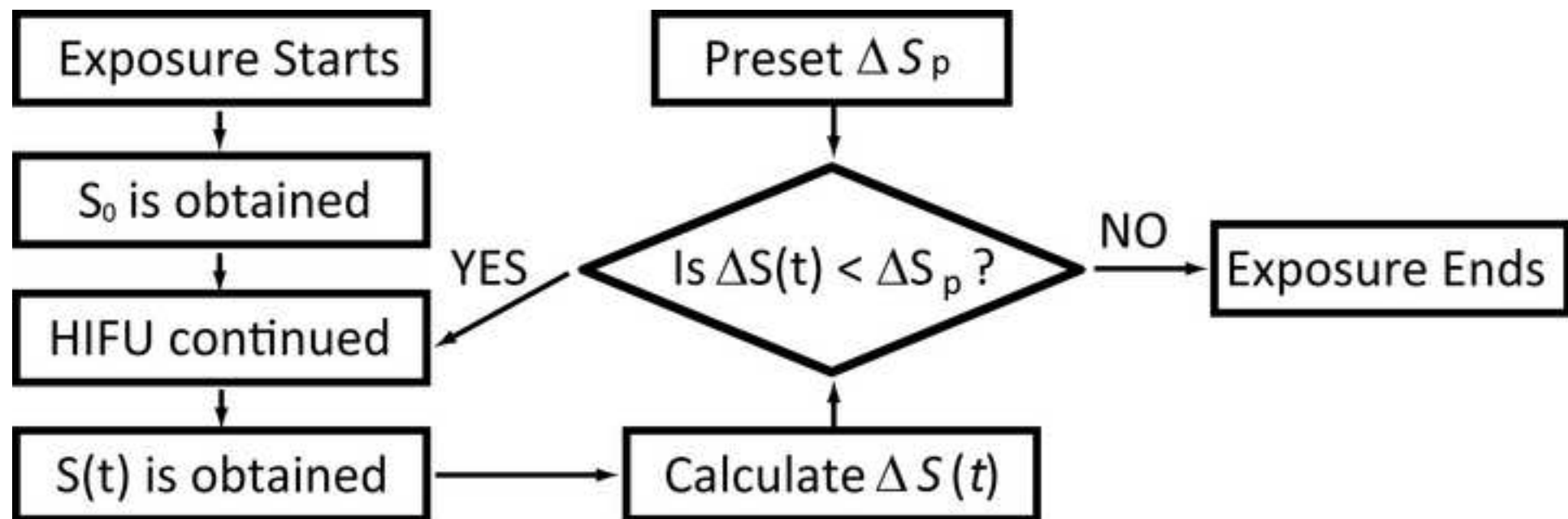


Figure 8
[Click here to download high resolution image](#)

